

## Supporting Information

# Dual Ligand Enabled Non-Directed C–H Chalcogenation of Arenes and Heteroarenes

Soumya Kumar Sinha<sup>1†</sup>, Subir Panja<sup>1†</sup>, Jagrit Grover<sup>1†</sup>, Partha Sarathi Hazra<sup>1</sup>,  
Saikat Pandit<sup>1</sup>, Yogesh Bairagi<sup>1</sup>, Xinglong Zhang<sup>2\*</sup>, Debabrata Maiti<sup>1\*</sup>

<sup>[1]</sup> Department of Chemistry, Indian Institute of Technology Bombay, Powai, Mumbai  
400076, India.

<sup>[2]</sup> Institute of High Performance Computing, Agency for Science, Technology and Research  
(A\*STAR), 1 Fusionopolis Way, #16–16 Connexis, Singapore, 138632, Singapore.

E-mail:

Debabrata Maiti: [dmaiti@chem.iitb.ac.in](mailto:dmaiti@chem.iitb.ac.in)

Xinglong Zhang: [zhang\\_xinglong@ihpc.a-star.edu.sg](mailto:zhang_xinglong@ihpc.a-star.edu.sg)

## **Computational Section- Part II**

## 6. Computational Methods.

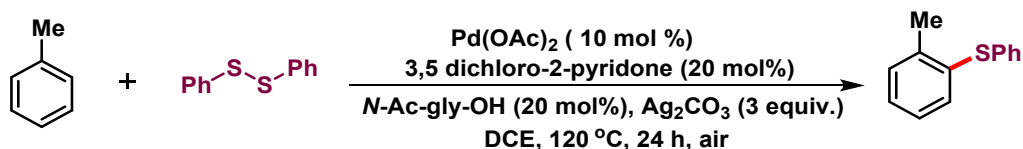
Density functional theory (DFT) calculations were performed with *Gaussian 16* rev. B.01.<sup>1</sup> Geometry optimizations were initially performed using the global-hybrid meta-NGA (nonseparable gradient approximation) MN15 functional<sup>2</sup> with the def2-SVP<sup>3,4</sup> Karlsruhe-family basis set and the optimized structures further refined with a mix of larger basis set consisting of triple- $\zeta$  valence def2-TZVPD (where ‘D’ indicates diffuse basis functions) for Pd<sup>5,6</sup> and Ag<sup>5,6</sup> atoms and def2-SVP<sup>3,4</sup> for all other atoms (BS1). MN15 functional was chosen as it performs much better than many other functionals (e.g.  $\omega$ B97X-D and TPSS) in predicting transition metal (TM) reaction barrier heights and giving better geometries for both TM complexes and organic molecules.<sup>2</sup> Minima and transition structures on the potential energy surface (PES) were confirmed using harmonic frequency analysis at the same level of theory, showing respectively zero and one imaginary frequency. Where appropriate for cases where visual inspection of TS imaginary frequency is not obvious, intrinsic reaction coordinate (IRC) analyses<sup>7,8</sup> were performed to confirm that the found TSs connect to the right reactants and products. Single point (SP) corrections were performed using MN15 functional and def2-QZVP<sup>3</sup> basis set for all atoms. The SMD implicit continuum solvation model<sup>9</sup> was used to account for the effect of dichloroethane (DCE) solvent on the computed Gibbs energy profile. Gibbs energies were evaluated at the reaction temperature of 393.15 K (120°C), using a quasi-RRHO treatment of vibrational entropies.<sup>10,11</sup> Vibrational entropies of frequencies below 100 cm<sup>-1</sup> were obtained according to a free rotor description, using a smooth damping function to interpolate between the two limiting descriptions. The free energies were further corrected using standard concentration of 1 mol/L, which were used in solvation calculations. Unless otherwise stated, the final SMD (dichloroethane)-MN15/def2-QZVP//MN15/BS1 Gibbs energies are used for discussion throughout. *All Gibbs energy values in the text and figures are quoted in kcal mol<sup>-1</sup>.*

Non-covalent interactions (NCIs) were analyzed using NCIPLOT<sup>12</sup> calculations. The *.wfn* files for NCIPLOT were generated at MN15/DGDZVP<sup>13,14</sup> level of theory. NCI indices calculated with NCIPLOT were visualized at a gradient isosurface value of  $s = 0.5$  au. These are colored according to the sign of the second eigenvalue ( $\lambda_2$ ) of the Laplacian of the density ( $\nabla^2\rho$ ) over the range of -0.1 (blue = attractive) to +0.1 (red = repulsive). Molecular orbitals are visualized using an isosurface value of 0.05 au throughout. All molecular structures and molecular orbitals were visualized using *PyMOL* software.<sup>15</sup>

Geometries of all optimized structures (in .xyz format with their associated energy in Hartrees) are included in a separate folder named *structures\_xyz* with an associated README file. All these data have been deposited with this Supporting Information.

## 7. Model reaction

For computational modeling, we have chosen the following reaction (Scheme S1) for mechanistic studies.



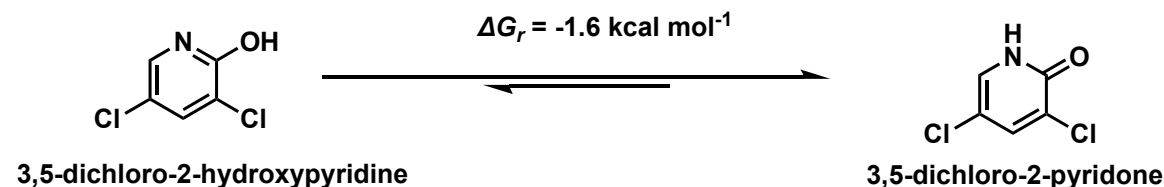
**Scheme S1.** Model reaction used for computational mechanistic studies.

### 7.1 Conformational considerations

Diphenylsulfane guess rotamers were generated by varying the C-S-S-C dihedral angles. The resultant rotamers were pre-optimized using the GFN2-xTB<sup>16</sup> extended semiempirical tight-binding method in the *xtb* program<sup>17,18</sup> from Grimme's group. The resultant distinct clusters were further optimized using DFT and the lowest energy structure is used throughout.

### 7.2 Ligand tautomerism

The equilibrium between the two tautomeric forms of the pyridone ligand is computed. It was found that 3,5-dichloro-2-pyridone is 1.6 kcal mol<sup>-1</sup> more stable than 3,5-dichloro-2-hydroxypyridine (Scheme S2). For structures involving either tautomer in the Gibbs energy profile calculation, the energy of the most stable form of the ligand (i.e., 3,5-dichloro-2-pyridone) is used.

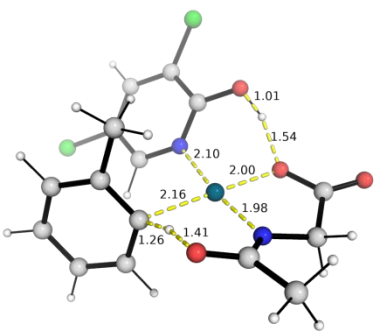
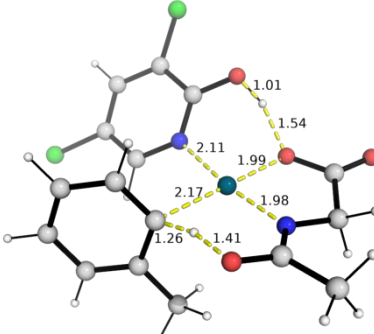
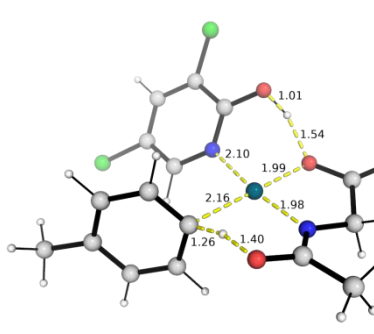
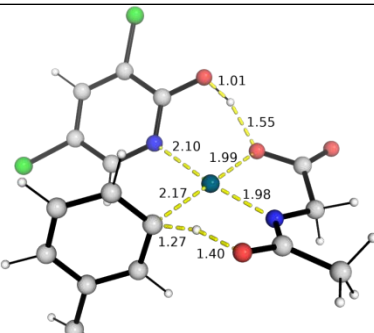
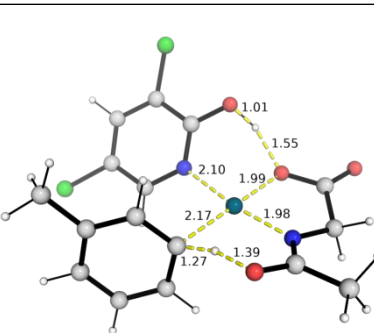


**Scheme S2.** Model reaction used for computational mechanistic studies.

## 8. C–H activation transition states (TSs)

### 8.1 C–H activation TSs using MPAA *N*-acetylglycine as internal base, with 3,5 dichloro-2-hydroxypyridine as co-ligand

The transition states for the concerted metalation deprotonation (CMD) C–H activation step with MPAA as internal base involving 3,5-dichloro-2-hydroxypyridine co-ligand is shown in Figure S1. For *ortho*- and *meta*-C–H activation TSs, both conformers were considered. The TS for the activation of *ortho*-C–H bond (**o-TS1**) has the lowest activation barrier, at 21.3 kcal mol<sup>-1</sup>; the TS for the activation of *para*-C–H bond (**p-TS1**) is 1.3 kcal mol<sup>-1</sup> higher, at 22.6 kcal mol<sup>-1</sup> whereas the TS for the activation of *meta*-C–H bond (**m-TS1**) is 2.0 kcal mol<sup>-1</sup> higher, at 23.3 kcal mol<sup>-1</sup>.

<b>o-TS1</b>	<b>o-TS1-c2</b>	<b>p-TS1</b>
$\Delta G^\ddagger = 21.3 \text{ kcal mol}^{-1}$	22.2 kcal mol <sup>-1</sup>	22.6 kcal mol <sup>-1</sup>
		
<b>m-TS1</b>	<b>m-TS1-c2</b>	
$\Delta G^\ddagger = 23.3 \text{ kcal mol}^{-1}$	23.5 kcal mol <sup>-1</sup>	
		

**Figure S1.** DFT optimized transition state structures for the C–H activation of toluene with 3,5 dichloro-2-hydroxypyridine co-ligand. Activation barriers are taken relative to the sum of starting materials.

Figure S2 shows the HOMO structures and the non-covalent interaction (NCI) plots for the lowest barrier regioselective C–H activation TSs. The HOMO structures show similar electronic distribution, suggesting similar orbital interactions in these TSs. For the NCI plots, there seems to be more favourable interactions in the TS for the activation of *ortho*-C–H bond

(circled in cyan) compared to the other two positions, although a quantitative comparison is difficult given these plots.

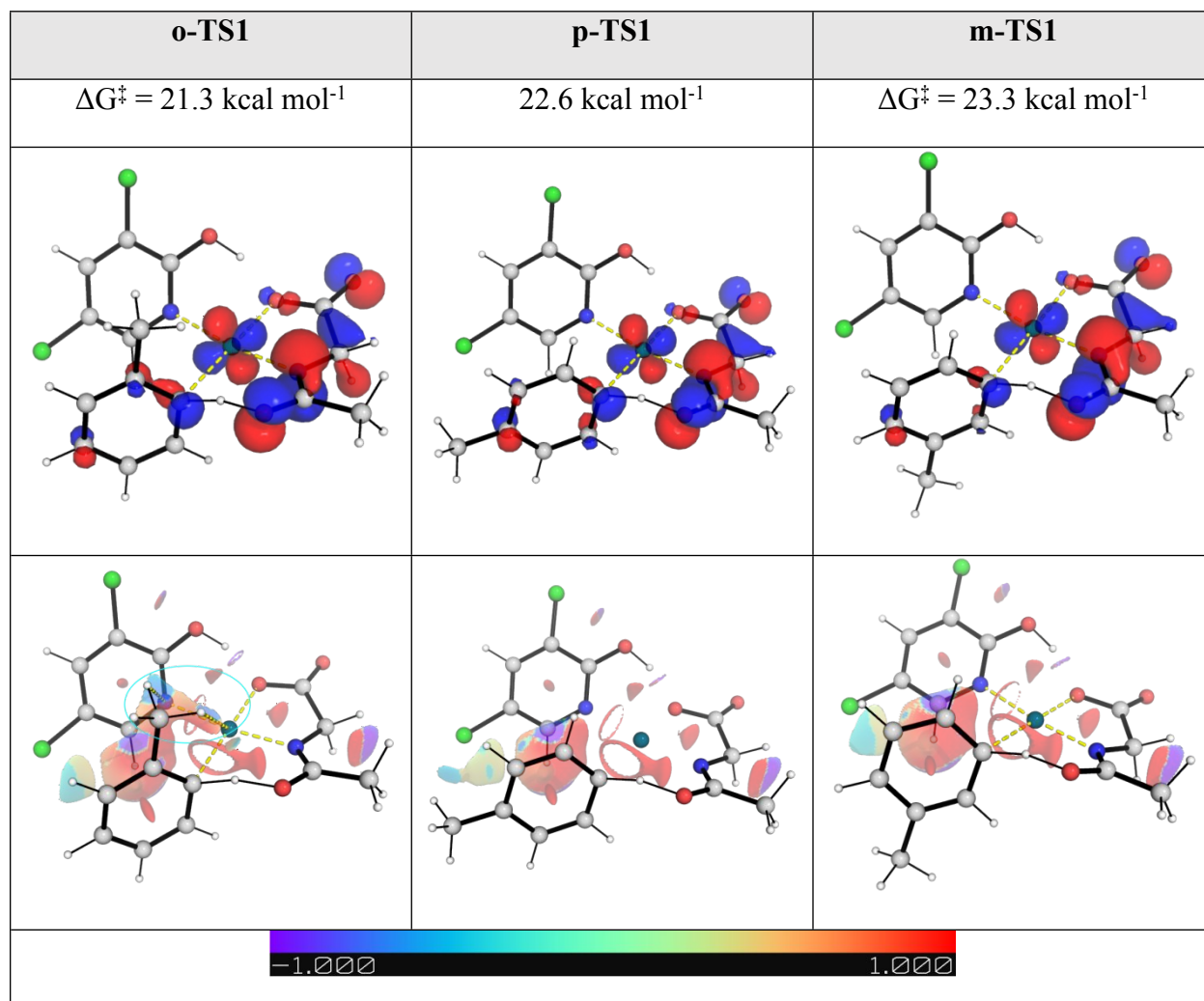


**Figure S2.** HOMO and NCI plots for the C–H activation of toluene using MPAA as internal base, with 3,5 dichloro-2-hydroxypyridine co-ligand. HOMOs are plotted at an isosurface value of 0.05 au.

We further carried out the distortion-interaction<sup>19,20</sup>/activation strain<sup>20–24</sup> (DI–AS) analysis on the key TSs to discern the factors affecting regioselectivity in the C–H activation step. Geometries are taken from along the IRC reaction coordinate at every 3<sup>rd</sup> point interval and single point solvent-phase calculations were performed at SMD (dichloroethane)-MN15/def2-QZVP level of theory to obtain DI-AS profiles, shown in Figure S3 below. From the DI-AS plot, we see that the TS for the activation of the *ortho*-C–H bond is lowest due to more favourable interaction energies along the IRC, while the strain energies are similar for all three TSs.

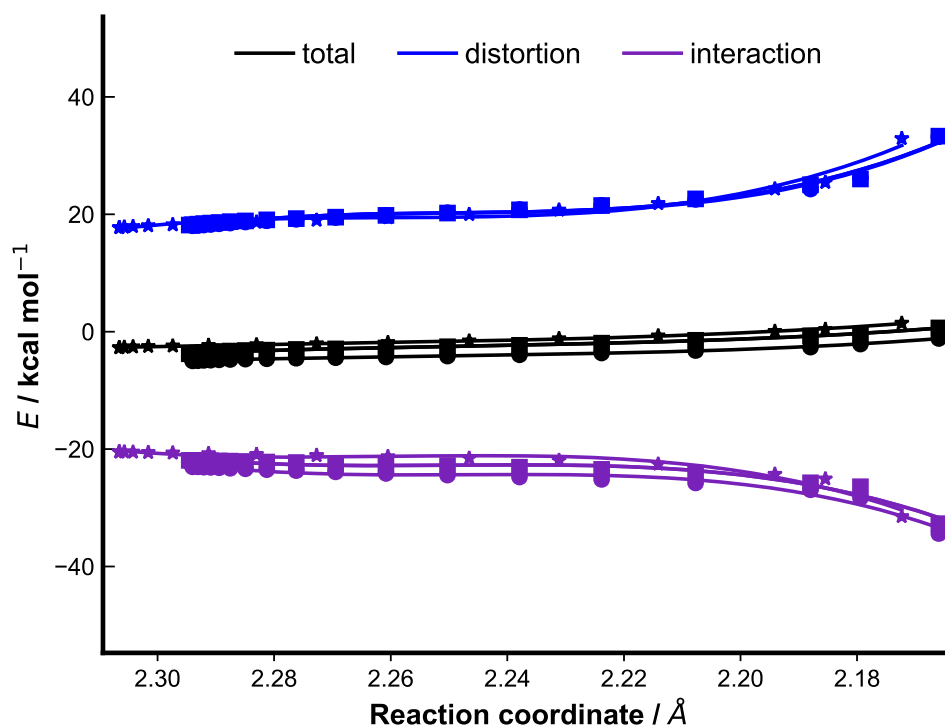


**Figure S3.** The activation strain or distortion-interaction analyses applied to the IRC paths along the rate-determining C–H activations transition states. All energies are calculated at SMD (dichloroethane)-MN15/def2-QZVP and used without any further corrections. Circle markers are points along *ortho*-C–H activation TS; star markers are points along *meta*-C–H activation TS; square markers are points along *para*-C–H activation TS.

## 8.2 C–H activation TSs using MPAA *N*-acetylglycine as internal base, with 3,5 dichloro-2-pyridone as co-ligand

The transition states for the concerted metalation deprotonation (CMD) C–H activation step with MPAA as internal base involving 3,5-dichloro-2-pyridone co-ligand is shown in Figure S4. For *ortho*- and *meta*-C–H activation TSs, the corresponding lowest energy conformer from section 1.4.2 previously was used. The TS for the activation of *ortho*-C–H bond (**o-TS1'**) is at 24.2 kcal mol<sup>-1</sup> while that for *para*-C–H bond (**p-TS1'**) is at 25.5 kcal mol<sup>-1</sup> and that for *meta*-C–H bond (**m-TS1'**) is at 26.6 kcal mol<sup>-1</sup>. All these TSs have higher barriers than the corresponding TSs using 3,5-dichloro-2-hydroxypyridine as the coordinating ligand (Figure S1). This is potentially due to the better electron-donating ability of the lone pair on the N atom rather than from the O atom, allowing the TSs in Figure S1 (ligand in 3,5-dichloro-2-hydroxypyridine form) to be stabilised to a larger extent than those in Figure S4 (ligand in 3,5-dichloro-2-pyridone form).

<b>o-TS1'</b>	<b>p-TS1'</b>	<b>m-TS1'</b>
24.2 kcal mol <sup>-1</sup>	$\Delta G^\ddagger = 25.5$ kcal mol <sup>-1</sup>	26.6 kcal mol <sup>-1</sup>

**Figure S4.** DFT optimized transition state structures for the C–H activation of toluene with 3,5 dichloro-2-pyridone co-ligand. Activation barriers are taken relative to the sum of starting materials.

### 8.3 C–H activation TSs using deprotonated pyridone ligand as internal base, with MPAA as co-ligand

The transition states for the concerted metalation deprotonation (CMD) C–H activation step with deprotonated pyridone ligand as internal base involving N-acetylglycine co-ligand is shown in Figure S5. The TS for the activation of *ortho*-C–H bond (**o-TS1''**) is at 26.6 kcal mol<sup>-1</sup> while that for *para*-C–H bond (**p-TS1''**) is at 26.8 kcal mol<sup>-1</sup> and that for *meta*-C–H bond (**m-TS1''**) is at 27.8 kcal mol<sup>-1</sup>. All these TSs have higher barriers than the corresponding TSs using MPAA N-acetylglycine as internal base and 3,5-dichloro-2-hydroxypyridine as the coordinating ligand (Figure S1).

<b>o-TS1''</b>	<b>p-TS1''</b>	<b>m-TS1''</b>
26.6 kcal mol <sup>-1</sup>	26.8 kcal mol <sup>-1</sup>	27.8 kcal mol <sup>-1</sup>
<b>m-TS1''-c2</b>	<b>o-TS1''-c2</b>	
$\Delta G^\ddagger = 27.8$ kcal mol <sup>-1</sup>	$\Delta G^\ddagger = 28.0$ kcal mol <sup>-1</sup>	



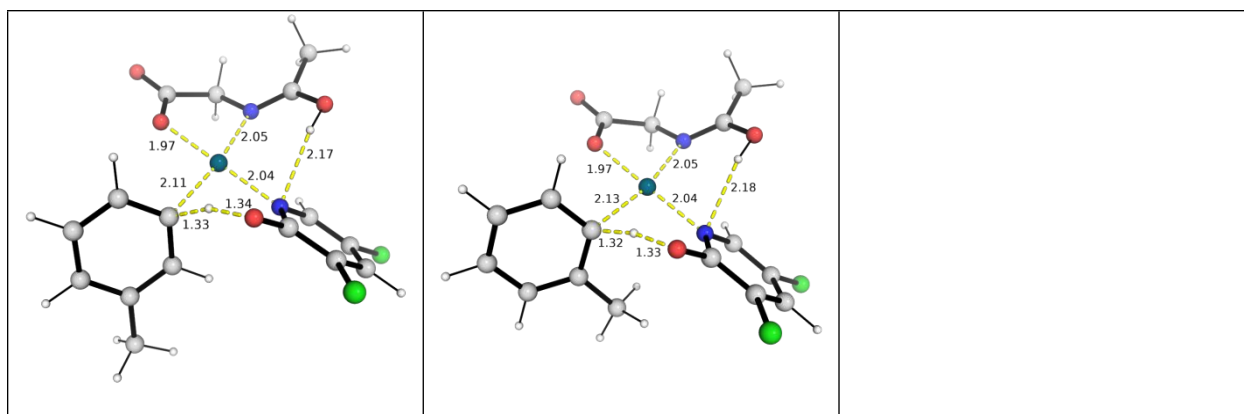


**Figure S5.** DFT optimized transition state structures for the C–H activation of toluene using pyridone as internal base and N-acetylglycine as co-ligand. Activation barriers are taken relative to the sum of starting materials.

#### 8.4 C–H activation TSs using tert-butylbenzene substrate

The DFT-optimized TSs for C–H activation step utilizing tert-butyl benzene substrate and the associated relative activation barriers are shown in Figure S6. For *ortho*- and *meta*-C–H activation TSs, both conformers were considered. The TS for the activation of *meta*-C–H bond (**m-TS1-tbz**) has the lowest activation barrier; the TS for the activation of *para*-C–H bond (**p-TS1-tbz**) is 0.5 kcal mol<sup>-1</sup> higher whereas the TS for the activation of *ortho*-C–H bond (**m-TS1**) is 1.2 kcal mol<sup>-1</sup> higher. These findings are consistent with the computed relative barriers for the C–H activation of tert-butyl benzene substrate as reported by van Gemmeren and co-workers.<sup>25</sup>

<b>m-TS1-tbz</b>	<b>m-TS1-tbz-c2</b>	<b>p-TS1-tbz</b>
$\Delta\Delta G^\ddagger = 0.0 \text{ kcal mol}^{-1}$	0.3 kcal mol <sup>-1</sup>	0.5 kcal mol <sup>-1</sup>
<b>o-TS-tbz</b>	<b>m-TS1-tbz-c2</b>	
$\Delta\Delta G^\ddagger = 1.2 \text{ kcal mol}^{-1}$	2.6 kcal mol <sup>-1</sup>	

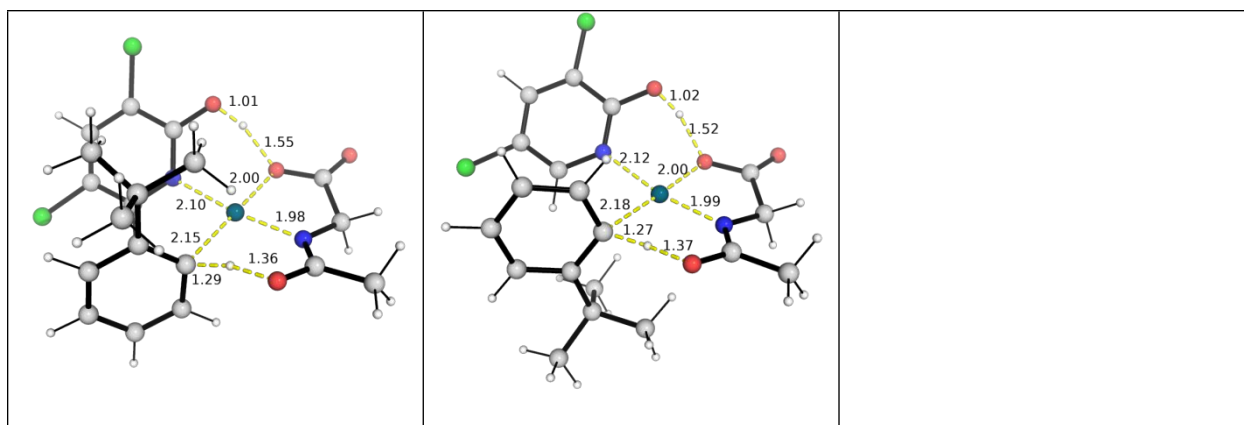


**Figure S6.** DFT optimized transition state structures for the C–H activation of tert-butyl benzene substrate with 3,5 dichloro-2-hydroxypyridine co-ligand. Activation barriers are taken relative to the lowest energy TS.

## 9. Oxidative addition/insertion transition states (TSs)

We considered all the possibilities for the oxidative addition (OA) of diphenyl disulfide substrate into Pd-centre. The mechanistic possibilities for the OA step involving neutral, cationic and anionic Pd-species are shown in Figures S7, S8 and S9 respectively. The OA step into Pd(OAc)<sub>2</sub> species before C–H activation step was also considered (Figure S10). All these possibilities (OA with different combinations/arrangements of ligands) suggest that the oxidative addition mechanism has very high barriers. In addition, these barriers are all higher than the C–H activation step, inconsistent with the experimental observation that the C–H activation step is the turnover-frequency-determining transition state (TDTS).

### 9.1 Mechanistic possibilities for the OA step involving neutral Pd-species

Starting from the *ortho*-C–H activated complex, we first consider the insertion where the MPAA ligand loses one coordination side on Pd-centre, giving a vacant site for diphenyl disulfide coordination and subsequent insertion. We found that these TSs have a barrier of 39.5 kcal mol<sup>-1</sup> (**OA-1**) and 40.6 kcal mol<sup>-1</sup> (**OA-2**).

We next consider the OA of diphenyl disulfide substrate into the *ortho*-C–H activated complex where the pyridone ligand is lost from the coordination, with only MPAA present in the OA TSs (**OA-3** and **OA-4**). These TSs also have high barriers with **OA-3** at 37.8 kcal mol<sup>-1</sup> while **OA-4** is at 35.8 kcal mol<sup>-1</sup>.

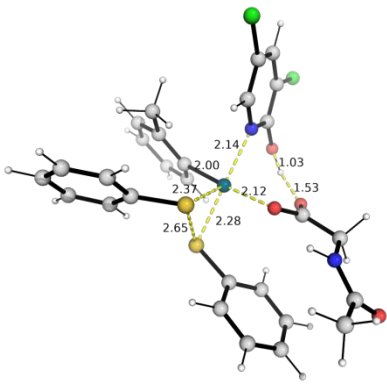
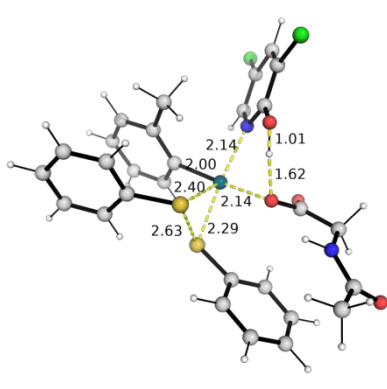
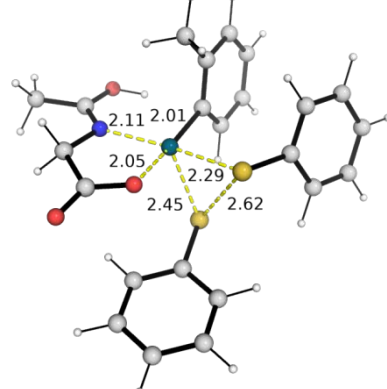
Next, we consider the OA TSs where the MPAA ligand is lost from coordination while the pyridone ligand remains. These TSs also have rather high barrier, with **OA-5** at 34.2 kcal mol<sup>-1</sup> and **OA-6** at 36.3 kcal mol<sup>-1</sup>.

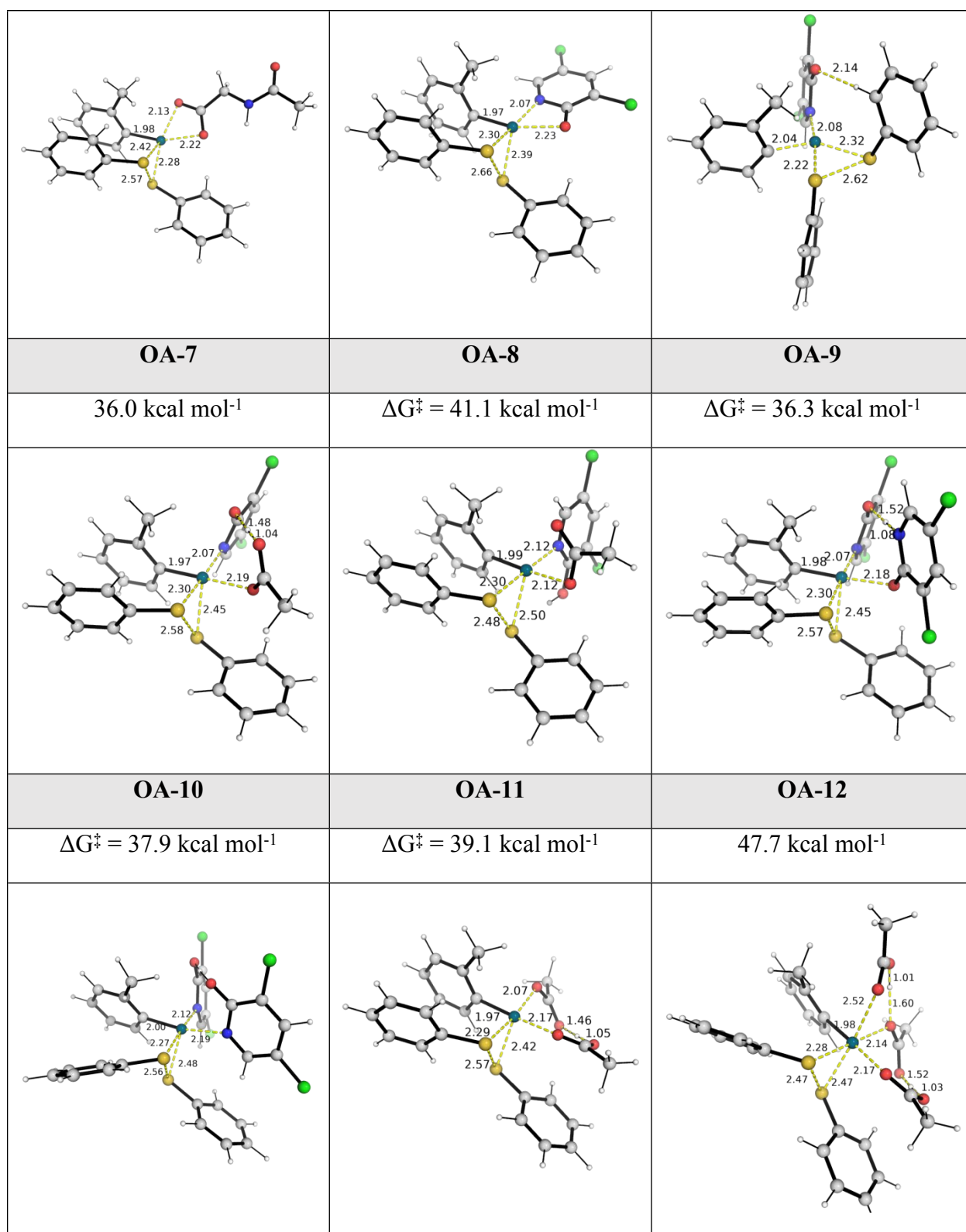
Next, from the *ortho*-C–H activated complex, we consider the OA TSs where an acetate ligand replaces the MPAA ligand. These TSs again have high barriers, with **OA-7** at 36.0 kcal mol<sup>-1</sup> and **OA-8** at 41.1 kcal mol<sup>-1</sup>.

We also consider the OA TSs in which another pyridone ligand replaces the MPAA ligand (**OA-9** and **OA-10**). These also have high barriers, with **OA-9** at 36.3 kcal mol<sup>-1</sup> and **OA-10** at 37.9 kcal mol<sup>-1</sup>.

Next, we consider the OA TSs in which the acetate molecules replace both the pyridone ligand and the MPAA ligand. For Pd-species undergoing OA with two acetates (**OA-11**), the barrier is at 39.1 kcal mol<sup>-1</sup>; the TS with three acetates (**OA-12**) has the barrier is at 47.7 kcal mol<sup>-1</sup>.

All these computed barriers suggest that the oxidative insertion of diphenyl disulfide into the C–H activated Pd-species is difficult and unlikely to be the actual mechanism.

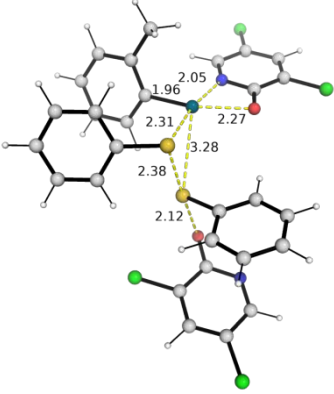
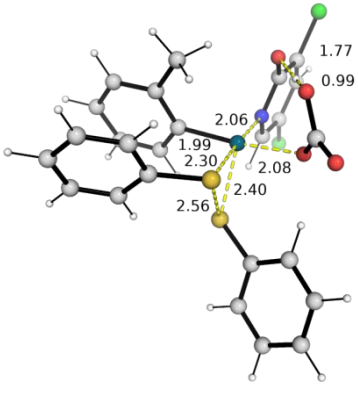
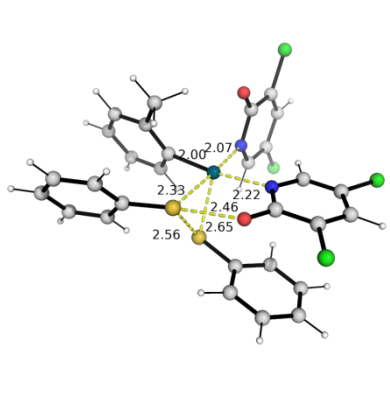
Neutral OA TSs		
OA-1	OA-2	OA-3
39.5 kcal mol <sup>-1</sup>	40.6 kcal mol <sup>-1</sup>	37.8 kcal mol <sup>-1</sup>
		
OA-4	OA-5	OA-6
35.8 kcal mol <sup>-1</sup>	$\Delta G^\ddagger = 34.2$ kcal mol <sup>-1</sup>	36.3 kcal mol <sup>-1</sup>



**Figure S7.** DFT optimized transition state structures for the oxidative addition of diphenyl disulfide into neutral Pd-species. Activation barriers are taken relative to the sum of starting materials.

## 9.2 Mechanistic possibilities for the OA step involving anionic Pd-species

The OA step involving anionic Pd-species was also considered. The results are shown in Figure S8. These TSs have barriers that are also quite high. **OA-1'** starting guess structure has the anionic pyridone N-atom coordinating to Pd, however, it proves to be unfavorable for it to stay coordinated – geometry optimization moves the anionic pyridone molecule away from the Pd-center. Comparing **OA-1'** and **OA-3'**, it looks like having the pyridone anion coordinated to Pd is less favorable than having it away from the Pd center. Nevertheless, these barriers are all higher than the TDTS C–H activation step and are less likely to be the mechanism.

Anionic OA TSs		
OA-1'	OA-2'	OA-3'
$\Delta G^\ddagger = 29.1 \text{ kcal mol}^{-1}$	31.8 kcal mol <sup>-1</sup>	36.1 kcal mol <sup>-1</sup>
		

**Figure S8.** DFT optimized transition state structures for the oxidative addition of diphenyl disulfide into anionic Pd-species. Activation barriers are taken relative to the sum of starting materials.

### 9.3 Mechanistic possibilities for the OA step involving cationic Pd-species

The OA step involving cationic Pd-species was also considered. The result is shown in Figure S9. The cationic OA insertion TS has a very high barrier of 67.5 kcal mol<sup>-1</sup>.

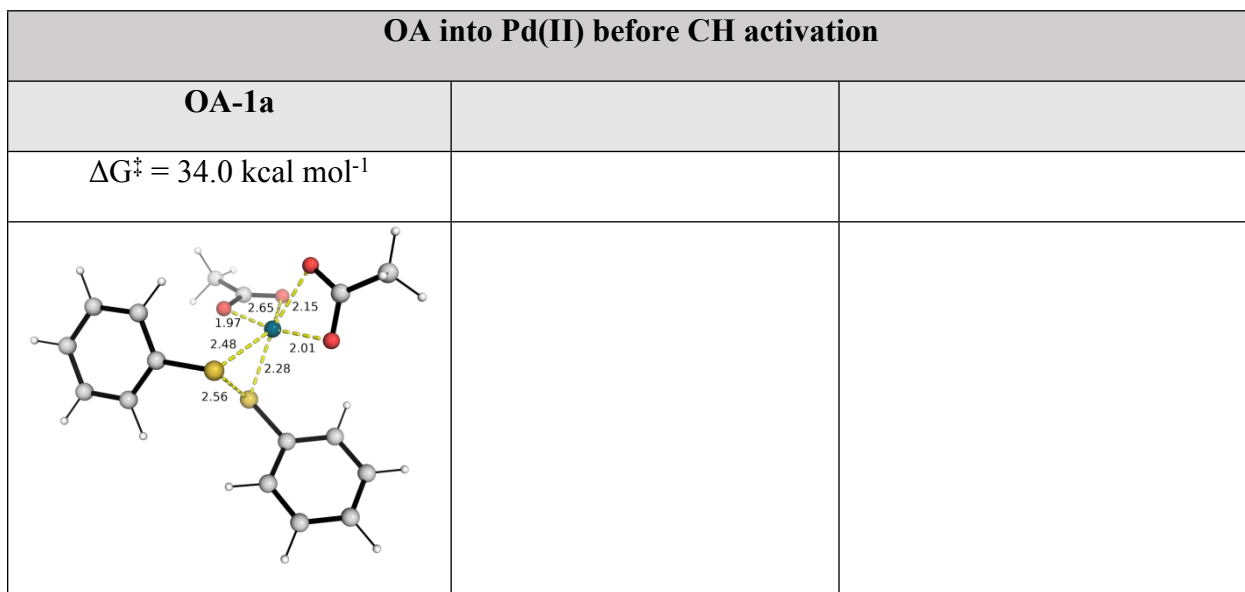
Cationic OA TSs		
OA-1''		
$\Delta G^\ddagger = 67.5 \text{ kcal mol}^{-1}$		



**Figure S9.** DFT optimized transition state structures for the oxidative addition of diphenyl disulfide into cationic Pd-species. Activation barriers are taken relative to the sum of starting materials.

#### 9.4 Mechanistic possibilities for the OA step into Pd(OAc)<sub>2</sub> species before C–H activation step

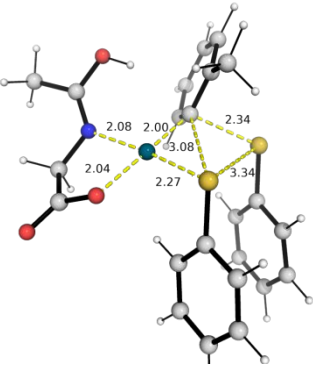
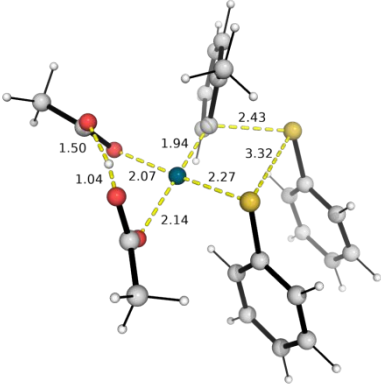
The OA step into Pd(OAc)<sub>2</sub> species before C–H activation step was also considered. This TS (**OA-1a**, Figure S10) has a high barrier of 34.0 kcal mol<sup>-1</sup>. Oxidative insertion into Pd(II) catalyst before CH activation step is less likely as this barrier is higher than firstly CH activation step as shown in Figure S1.



**Figure S10.** DFT optimized transition state structures for the oxidative addition of diphenyl disulfide into Pd(OAc)<sub>2</sub> species before C–H activation step. Activation barriers are taken relative to the sum of starting materials.

#### 10. Migratory insertion transition states (TSs)

The alternative migratory insertion (MI) of diphenyl disulfide substrate into C–H activated Pd-species was also considered. These TSs (Figure S11) have very high barriers and the MI step is unlikely the mechanism for the present reaction.

Migratory insertion TSs		
MI-1	MI-2	
$\Delta G^\ddagger = 57.2 \text{ kcal mol}^{-1}$	$55.7 \text{ kcal mol}^{-1}$	
		

**Figure S11.** DFT optimized transition state structures for the migratory insertion of diphenyl disulfide into C–H activated species. Activation barriers are taken relative to the sum of starting materials.

## 11. Transmetalation pathways

### 11.1 Oxidative insertion into Ag catalyst species

The oxidative insertion of diphenyl disulfide into Ag catalyst was considered. The energy profiles for the insertion into  $\text{Ag}_2\text{CO}_3$  and  $\text{AgOAc}$  are shown in Figure S12. The insertion of diphenyl disulfide into  $\text{Ag}_2\text{CO}_3$  has lower activation barrier of  $22.2 \text{ kcal mol}^{-1}$  compared to the insertion into  $\text{AgOAc}$ , which has a barrier of  $25.5 \text{ kcal mol}^{-1}$ .

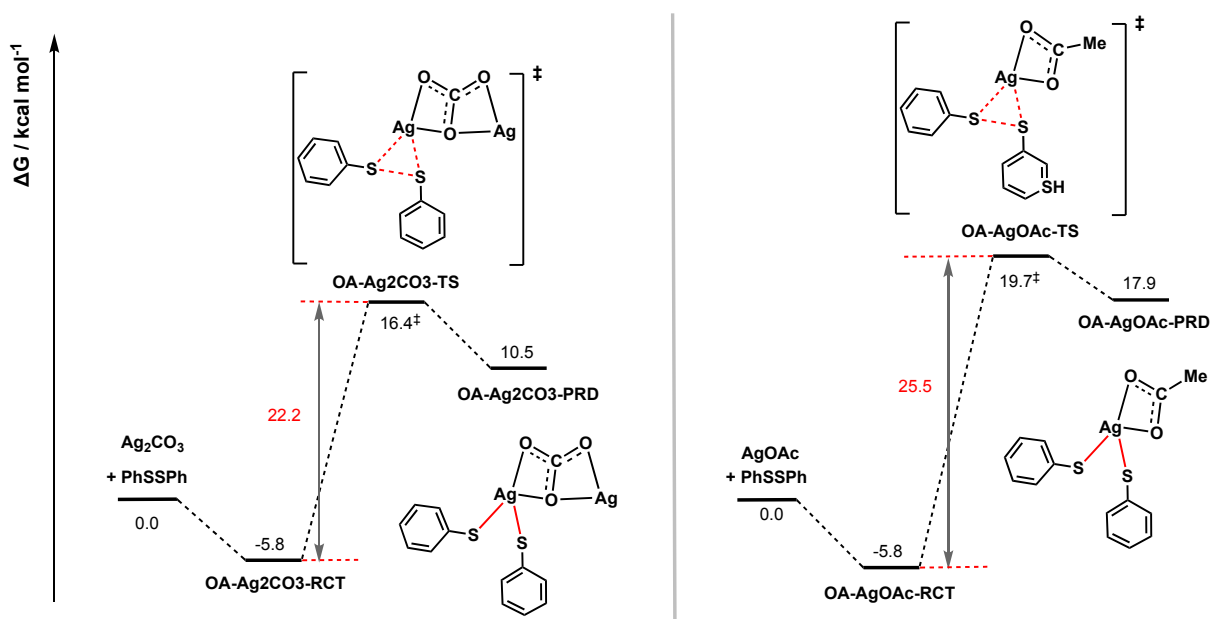
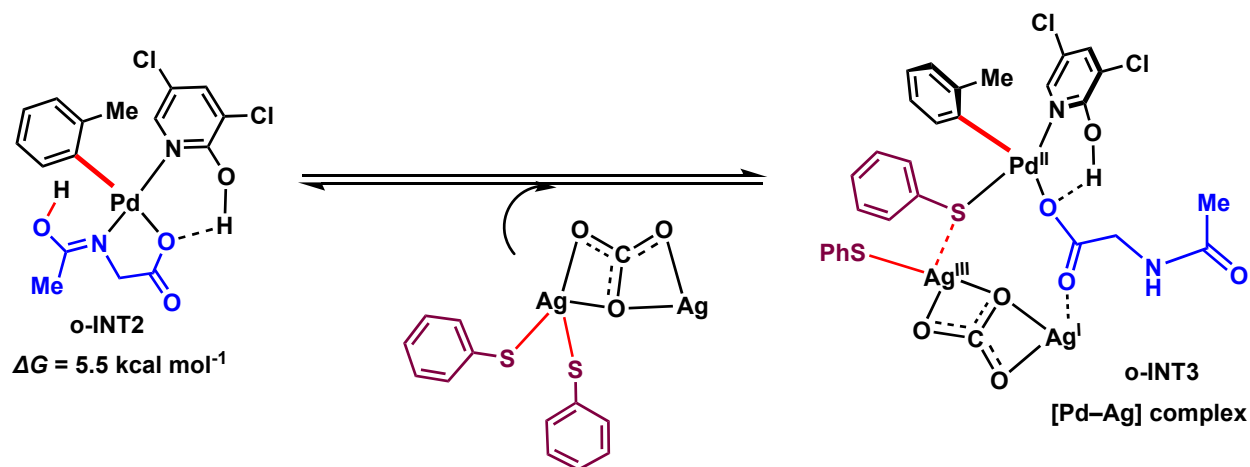


**Figure S12.** Gibbs energy profile for the insertion of diphenyl disulfide into Ag catalyst species.

## 11.2 Transmetalated Pd-Ag species

The diphenyl disulfide inserted silver complex can undergo a transmetalation-like process in which a PhS-group is transferred from the Ag-centre to the Pd-centre (Scheme S3). The resulting complex is optimized, taking into account of various isomers that can be formed (Figure S13). This [Pd–Ag] complex formation is exergonic and may be possible to occur.



**Scheme S3.** Formation of [Pd–Ag] complex with the formation of Pd–SPh bond.

<b>o-INT3</b>	<b>o-INT3-c2</b>	<b>o-INT3-c3</b>
$\Delta G = 1.8 \text{ kcal mol}^{-1}$	$\Delta G = 4.7 \text{ kcal mol}^{-1}$	$\Delta G = 4.9 \text{ kcal mol}^{-1}$
<b>o-INT3-c4</b>	<b>o-INT3-c5</b>	<b>o-INT3-c6</b>
$\Delta G = 5.8 \text{ kcal mol}^{-1}$	$\Delta G = 6.3 \text{ kcal mol}^{-1}$	$\Delta G = 8.0 \text{ kcal mol}^{-1}$



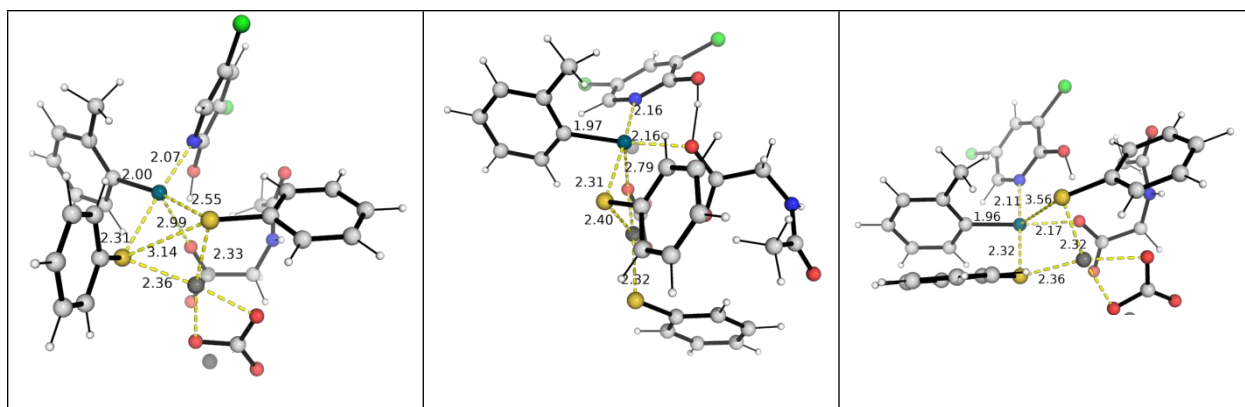


**Figure S13.** DFT optimized structures for possible isomers of [Pd–Ag] complex. Gibbs energies are taken relative to the sum of starting materials.

## 12. Reductive elimination step

The DFT optimized structures for the reductive elimination step forming the sulfane product is shown in Figure S14. This step has a very low barrier of 2.6 kcal mol<sup>-1</sup> from the transmetalated Pd–Ag complex **o-INT3**. In addition, this step is highly exergonic, forming **o-INT4** at -10.2 kcal mol<sup>-1</sup> and is irreversible.

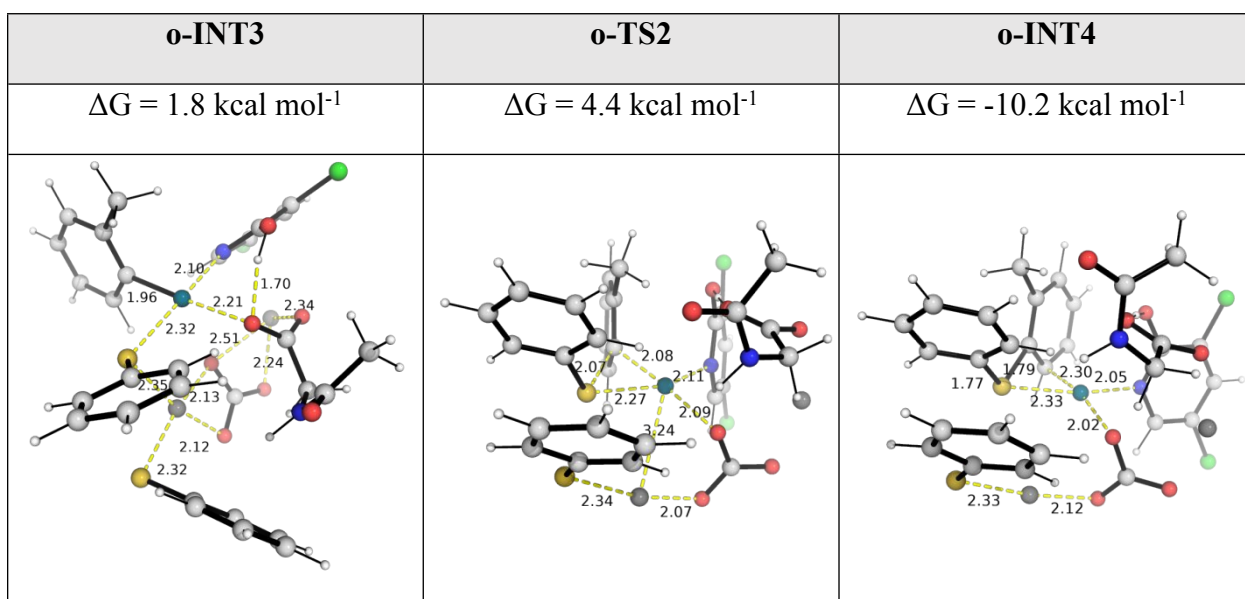


**Figure S14.** DFT optimized structures for the reductive elimination step, forming the sulfane product. Activation barriers are taken relative to the sum of starting materials.

## 13. Release of product

The possible reactions for the release of sulfane product show in Table S11 were computed. From the Gibbs energy of reaction, we can see that reaction **R1**, in which a dichlorohydroxypyridine

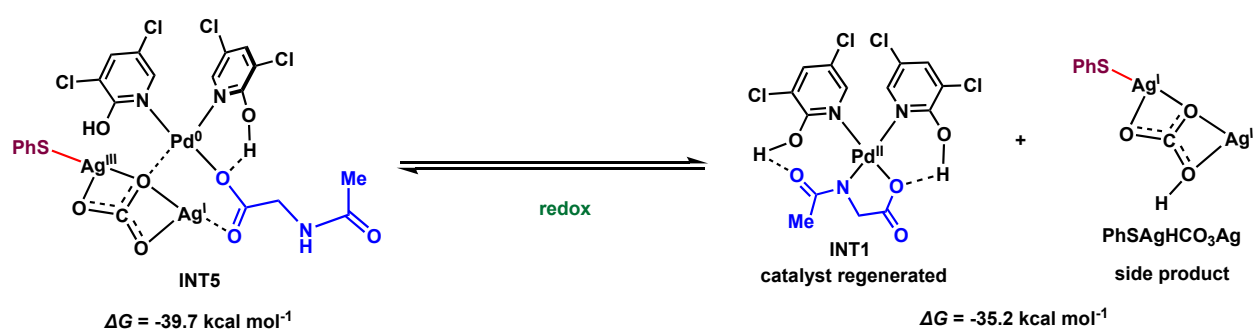
S/N	Reaction	$\Delta G_r /$ kcal mol <sup>-1</sup>
R1	<p>o-INT4 <math>\Delta G = -10.2</math> kcal mol<sup>-1</sup></p> <p>INT5 <math>\Delta G = -39.7</math> kcal mol<sup>-1</sup></p>	-29.5
R2	<p>o-INT4 <math>\Delta G = -10.2</math> kcal mol<sup>-1</sup></p> <p>INT5a <math>\Delta G = -26.8</math> kcal mol<sup>-1</sup></p>	-16.6
R3	<p>Pd(0)(dichloropyridine)<sub>2</sub></p> <p>Pd(0)(dichlorohydroxypyridine)<sub>2</sub></p>	-15.3
R4	<p>o-INT4 <math>\Delta G = -10.2</math> kcal mol<sup>-1</sup></p> <p>INT5b</p> <p>Pd(0)(dichlorohydroxypyridine)<sub>2</sub> <math>\Delta G = 28.3</math> kcal mol<sup>-1</sup></p>	38.5
R5	<p>o-INT4 <math>\Delta G = -10.2</math> kcal mol<sup>-1</sup></p> <p>PhSAgCO3AgMPAA</p> <p>Pd(0)(dichlorohydroxypyridine)<sub>2</sub> <math>\Delta G = 27.9</math> kcal mol<sup>-1</sup></p>	38.1

Table S11. Computed Gibbs energy of reaction for the release of sulfane product.

ligand displaces the sulfane product, is most exergonic and favourable. All other possibilities were less favoured thermodynamically.

#### 14. Regeneration of catalyst *via* redox

Scheme S4 shows the regeneration of active catalyst **INT1**, with the release of the side product, from **INT5**. This completes the reaction cycle as **INT1** subsequently carries out the second cycle of C–H activation of toluene substrate. This reaction has is thermodynamically uphill by 4.5 kcal mol<sup>-1</sup>.



**Scheme S4.** Redox chemistry to regenerate the activate Pd(II)-catalyst complex **INT1**.

#### 15. Optimized structures and absolute energies, zero-point energies

Geometries of all optimized structures (in .xyz format with their associated energy in Hartrees) are included in a separate folder named *final\_xyz* with an associated readme.txt file. All these data have been deposited and uploaded to zenodo.org (DOI: 10.5281/zenodo.6473595).

Absolute values (in Hartrees) for SCF energy, zero-point vibrational energy (ZPE), enthalpy and quasi-harmonic Gibbs free energy (at 120°C/393.15 K) for optimized structures are given below. Single point corrections in SMD dichloroethane using MN15/def2-QZVP level of theory are also included.

Structure	E/au	ZPE/au	H/au	T.S/au	qh-G/au	SP MN15/def2-QZVP
<b>dichloropyridon</b>						
e	-1241.531241	0.075518	-1241.4422	0.056518	-1241.498495	-1242.658717
<b>dichlorohydroxypyridine</b>						
	-1241.534533	0.075253	-1241.4458	0.056284	-1241.501935	-1242.656084

<b>HOAc</b>	-228.644533	0.062197	-228.57411	0.041723	-228.61541	-229.06955300
<b>Nacetylglucine</b>	-436.253431	0.118206	-436.12004	0.061666	-436.17856	-437.0589
<b>diphenylsulfane -c1</b>	-1258.182435	0.185397	-1257.9754	0.077159	-1258.048302	-1259.5116
<b>diphenylsulfane -c2</b>	-1258.182434	0.185402	-1257.9754	0.077087	-1258.048268	-1259.5116
<b>toluene</b>	-270.978507	0.128304	-270.83852	0.052789	-270.889069	-271.483625
<b>sulfane_product</b>	-899.481193	0.211292	-899.24815	0.075438	-899.320402	-900.642338
<b>acetate</b>	-228.059294	0.048219	-228.00312	0.04228	-228.044179	-228.581974
<b>PdOAc2_mono mer</b>	-583.809931	0.104326	-583.68809	0.068364	-583.753096	-584.645295
<b>carbonate</b>	-263.114881	0.014696	-263.09435	0.03674	-263.131093	-263.990498
<b>hydrogen_carbo nate</b>	-263.954044	0.027165	-263.92041	0.037775	-263.95818	-264.53534
<b>dichloropyridon e_anion</b>	-1240.978252	0.06161	-1240.9034	0.056248	-1240.959333	-1242.175766
<b>silver_acetate</b>	-374.748694	0.050631	-374.68765	0.052688	-374.738246	-375.185492
<b>silver_carbonat e</b>	-556.727692	0.017256	-556.6994	0.055206	-556.753788	-557.23599
<b>INT1-c2</b>	-3045.897064	0.249714	-3045.6038	0.129126	-3045.723633	-3048.914896
<b>INT1</b>	-3045.904173	0.248385	-3045.6124	0.129179	-3045.732411	-3048.919312
<b>o-INT1</b>	-2075.30424	0.301978	-2074.9602	0.124203	-2075.076122	-2077.710254
<b>o-TS1</b>	-2075.300574	0.297941	-2074.9614	0.120697	-2075.075154	-2077.703191
<b>o-INT2</b>	-2075.328504	0.303104	-2074.9835	0.124438	-2075.099178	-2077.73239
<b>o-TS1-c2</b>	-2075.29935	0.298015	-2074.9602	0.120293	-2075.073781	-2077.701938
<b>p-TS1</b>	-2075.297389	0.29771	-2074.9583	0.122341	-2075.072793	-2077.700357
<b>m-TS1</b>	-2075.295151	0.297641	-2074.956	0.123081	-2075.070707	-2077.699099
<b>m-TS1-c2</b>	-2075.296956	0.29781	-2074.9578	0.12099	-2075.071828	-2077.69953
<b>o-TS1'</b>	-2075.293472	0.297261	-2074.9545	0.124959	-2075.070573	-2077.696068
<b>p-TS1'</b>	-2075.290643	0.297012	-2074.9518	0.125693	-2075.068196	-2077.693603
<b>m-TS1'</b>	-2075.289724	0.297103	-2074.9508	0.124652	-2075.066822	-2077.692308
<b>o-TS1''</b>	-2075.280299	0.297519	-2074.9409	0.123248	-2075.05625	-2077.693388

<b>p-TS1''</b>	-2075.277323	0.297299	-2074.9379	0.126039	-2075.054419	-2077.692051
<b>m-TS1''</b>	-2075.276427	0.297352	-2074.937	0.12516	-2075.052979	-2077.690925
<b>m-TS1''-c2</b>	-2075.276104	0.297381	-2074.9367	0.125002	-2075.052607	-2077.690955
<b>o-TS1''-c2</b>	-2075.277067	0.297654	-2074.9377	0.122569	-2075.052475	-2077.691705
<b>OA-1</b>	-3333.504386	0.488399	-3332.9516	0.175313	-3333.11168	-3337.218941
<b>OA-2</b>	-3333.503976	0.489254	-3332.9505	0.172959	-3333.109426	-3337.219069
<b>OA-3</b>	-2091.924403	0.412273	-2091.4623	0.140157	-2091.592099	-2094.535308
<b>OA-4</b>	-2091.922895	0.41162	-2091.4604	0.146858	-2091.593983	-2094.535106
<b>OA-5</b>	-2897.209491	0.368631	-2896.7915	0.142346	-2896.922038	-2900.138164
<b>OA-6</b>	-2897.197782	0.367806	-2896.7801	0.1442	-2896.911985	-2900.133172
<b>OA-7</b>	-3125.896901	0.432044	-3125.4071	0.159664	-3125.553874	-3129.231227
<b>OA-8</b>	-3125.884104	0.43232	-3125.3935	0.162192	-3125.541639	-3129.222581
<b>OA-9</b>	-4138.790092	0.444906	-4138.2818	0.172609	-4138.43976	-4142.823632
<b>OA-10</b>	-4138.785231	0.44467	-4138.277	0.174234	-4138.435911	-4142.820018
<b>OA-11</b>	-2112.997973	0.419159	-2112.5268	0.146005	-2112.661819	-2115.633871
<b>OA-12</b>	-2341.670266	0.483562	-2341.1259	0.165995	-2341.278728	-2344.716051
<b>OA-1'</b>	-4138.257842	0.431185	-4137.7628	0.178003	-4137.923502	-4142.350059
<b>OA-2'</b>	-3161.255141	0.39812	-3160.8011	0.155308	-3160.944312	-3164.704798
<b>OA-3'</b>	-4138.25794	0.432072	-4137.7624	0.171764	-4137.920354	-4142.342129
<b>OA-1''</b>	-2897.591438	0.380336	-2897.1609	0.141483	-2897.291948	-2900.570625
<b>MI-1</b>	-2091.880643	0.411057	-2091.4194	0.139241	-2091.549654	-2094.503175
<b>MI-2</b>	-2112.964759	0.418241	-2112.4942	0.147036	-2112.630045	-2115.605964
<b>OA1a</b>	-1841.976653	0.289364	-1841.647	0.12417	-1841.759839	-1844.128462
<b>o-INT3</b>	-3890.355386	0.50805	-3889.77	0.205109	-3889.956475	-3894.530563
<b>o-INT3-c2</b>	-3890.355068	0.508072	-3889.7696	0.206122	-3889.956468	-3894.525731
<b>o-INT3-c3</b>	-3890.342641	0.509531	-3889.7564	0.204446	-3889.941795	-3894.527631
<b>o-INT3-c4</b>	-3890.339004	0.508355	-3889.7535	0.20688	-3889.940286	-3894.524034
<b>o-INT3-c5</b>	-3890.338264	0.507479	-3889.7535	0.206272	-3889.940389	-3894.52243
<b>o-INT3-c6</b>	-3890.339742	0.509043	-3889.7538	0.204522	-3889.939668	-3894.521978
<b>o-TS2</b>	-3890.350562	0.507478	-3889.7673	0.200896	-3889.950444	-3894.527686

<b>o-INT4</b>	-3890.365369	0.507798	-3889.7813	0.201848	-3889.965129	-3894.551044
<b>INT5</b>	-4232.469899	0.372719	-4232.0286	0.190955	-4232.200511	-4236.611729
<b>OA-Ag2CO3-RCT</b>	-1814.970465	0.203932	-1814.7325	0.110839	-1814.834526	-1816.784788
<b>OA-Ag2CO3-TS</b>	-1814.934978	0.203142	-1814.6984	0.112338	-1814.800248	-1816.748089
<b>OA-Ag2CO3-PRD</b>	-1814.940576	0.203824	-1814.7026	0.113395	-1814.805546	-1816.757834
<b>OA-AgOAc-RCT</b>	-1632.990324	0.237555	-1632.7196	0.105885	-1632.817855	-1634.734261
<b>OA-AgOAc-TS</b>	-1632.952354	0.236684	-1632.683	0.108998	-1632.781578	-1634.691826
<b>OA-AgOAc-PRD</b>	-1632.95382	0.237312	-1632.6832	0.108569	-1632.782245	-1634.695562
<b>Pd(0)(dichlorohydroxypyridine)2</b>	-2610.810229	0.152113	-2610.6275	0.101947	-2610.723115	-2613.043666
<b>Pd(0)(dichloropyridone)2</b>	-2610.775437	0.151945	-2610.5927	0.104184	-2610.689344	-2613.018295
<b>INT5a-c2</b>	-2990.867198	0.298235	-2990.5153	0.15655	-2990.657959	-2993.904456
<b>INT5a</b>	-2990.870863	0.297922	-2990.5194	0.155132	-2990.661044	-2993.905653
<b>INT5b</b>	-2521.031204	0.432438	-2520.5394	0.164159	-2520.689641	-2524.100421
<b>INT5b-c2</b>	-2521.016813	0.432271	-2520.5247	0.167188	-2520.676649	-2524.101074
<b>PhSAgCO3Ag MPAA</b>	-1621.505028	0.220161	-1621.2486	0.11317	-1621.354118	-1623.428967
<b>PhSAgCO3Ag MPAA-c2</b>	-1621.47822	0.218096	-1621.2223	0.123236	-1621.333841	-1623.415531
<b>PhSAgCO3Ag MPAA-c3</b>	-1621.477246	0.217408	-1621.2217	0.12529	-1621.334744	-1623.414986
<b>HCO3Ag</b>	-410.630056	0.028918	-410.59219	0.046966	-410.639012	-411.129522
<b>PhSAg</b>	-775.802216	0.092273	-775.69656	0.059677	-775.753935	-776.486407
<b>PhSAgHCO3Ag</b>	-1186.473506	0.122067	-1186.3276	0.091273	-1186.410754	-1187.650318

## 16. References:

### Full reference Gaussian 16:

Gaussian 16, Revision B.01, Frisch, M. J.; Trucks, G. W.; Schlegel, H. B.; Scuseria, G. E.; Robb, M. A.; Cheeseman, J. R.; Scalmani, G.; Barone, V.; Mennucci, B.; Petersson, G. A.; Nakatsuji, H.; Caricato, M.; Li, X.; Hratchian, H. P.; Izmaylov, A. F.; Bloino, J.; Zheng, G.; Sonnenberg, J. L.; Hada, M.; Ehara, M.; Toyota, K.; Fukuda, R.; Hasegawa, J.; Ishida, M.; Nakajima, T.; Honda, Y.; Kitao, O.; Nakai, H.; Vreven, T.; Montgomery Jr., J. A.; Peralta, J. E.; Ogliaro, F.; Bearpark, M.; Heyd, J. J.; Brothers, E.; Kudin, K. N.; Staroverov, V. N.; Kobayashi, R.; Normand, J.; Raghavachari, K.; Rendell, A.; Burant, J. C.; Iyengar, S. S.; Tomasi, J.; Cossi, M.; Rega, N.; Millam, J. M.; Klene, M.; Knox, J. E.; Cross, J. B.; Bakken, V.; Adamo, C.; Jaramillo, J.; Gomperts, R.; Stratmann, R. E.; Yazyev, O.; Austin, A. J.; Cammi, R.; Pomelli, C.; Ochterski, J. W.; Martin, R. L.; Morokuma, K.; Zakrzewski, V. G.; Voth, G. A.; Salvador, P.; Dannenberg, J. J.; Dapprich, S.; Daniels, A. D.; Farkas, Ö.; Foresman, J. B.; Ortiz, J. V.; Cioslowski, J.; Fox, D. J. Gaussian, Inc., Wallingford CT, 2016.

- [1] Frisch, M. J. .; Trucks, G. W. .; Schlegel, H. B. .; Scuseria, G. E. .; Robb, M. A. .; Cheeseman, J. R. .; Scalmani, G. .; Barone, V. .; Petersson, G. A. .; Nakatsuji, H. .; et al. Gaussian 16, Revision B.01. 2016.
- [2] Yu, H. S.; He, X.; Li, S. L.; Truhlar, D. G. MN15: A Kohn–Sham Global-Hybrid Exchange–Correlation Density Functional with Broad Accuracy for Multi-Reference and Single-Reference Systems and Noncovalent Interactions. *Chem. Sci.* **2016**, *7*, 5032–5051.
- [3] Weigend, F.; Ahlrichs, R. Balanced Basis Sets of Split Valence, Triple Zeta Valence and Quadruple Zeta Valence Quality for H to Rn: Design and Assessment of Accuracy. *Phys. Chem. Chem. Phys.* **2005**, *7*, 3297–3305.
- [4] Weigend, F. Accurate Coulomb-Fitting Basis Sets for H to Rn. *Phys. Chem. Chem. Phys.* **2006**, *8*, 1057–1065.
- [5] Rappoport, D.; Furche, F. Property-Optimized Gaussian Basis Sets for Molecular Response Calculations. *J. Chem. Phys.* **2010**, *133*, 134105.
- [6] Andrae, D.; Häußermann, U.; Dolg, M.; Stoll, H.; Preuß, H. Energy-Adjusted ab Initio

- Pseudopotentials for the Second and Third Row Transition Elements. *Theor. Chim. Acta* **1990**, *77*, 123–141.
- [7] Fukui, K. Formulation of the Reaction Coordinate. *J. Phys. Chem.* **2005**, *74*, 4161–4163.
- [8] Fukui, K. The Path of Chemical Reactions - The IRC Approach. *Acc. Chem. Res.* **1981**, *14*, 363–368.
- [9] Marenich, A. V.; Cramer, C. J.; Truhlar, D. G. Universal Solvation Model Based on Solute Electron Density and on a Continuum Model of the Solvent Defined by the Bulk Dielectric Constant and Atomic Surface Tensions. *J. Phys. Chem. B* **2009**, *113*, 6378–6396.
- [10] Grimme, S. Supramolecular Binding Thermodynamics by Dispersion-Corrected Density Functional Theory. *Chem.: Eur. J.* **2012**, *18*, 9955–9964.
- [11] Funes-Ardoiz, I.; Paton, R. S. GoodVibes v1.0.1 <http://doi.org/10.5281/zenodo.56091>.
- [12] Contreras-García, J.; Johnson, E. R.; Keinan, S.; Chaudret, R.; Piquemal, J. P.; Beratan, D. N.; Yang, W. NCIPLLOT: A Program for Plotting Noncovalent Interaction Regions. *J. Chem. Theory Comput.* **2011**, *7*, 625–632.
- [13] Sosa, C.; Andzelm, J.; Elkin, B. C.; Wimmer, E.; Dobbs, K. D.; Dixon, D. A. A Local Density Functional Study of the Structure and Vibrational Frequencies of Molecular Transition-Metal Compounds. *J. Phys. Chem.* **1992**, *96*, 6630–6636.
- [14] Godbout, N.; Salahub, D. R.; Andzelm, J.; Wimmer, E. Optimization of Gaussian-Type Basis Sets for Local Spin Density Functional Calculations. Part I. Boron through Neon, Optimization Technique and Validation. *Can. J. Chem.* **1992**, *70*, 560–571.
- [15] Schrödinger, L. *The PyMOL Molecular Graphics Development Component, Version 1.8*; 2015.
- [16] Bannwarth, C.; Ehlert, S.; Grimme, S. GFN2-XTB - An Accurate and Broadly Parametrized Self-Consistent Tight-Binding Quantum Chemical Method with Multipole Electrostatics and Density-Dependent Dispersion Contributions. *J. Chem. Theory Comput.* **2019**, *15*, 1652–1671.
- [17] Grimme, S.; Bannwarth, C.; Shushkov, P. A Robust and Accurate Tight-Binding



- Quantum Chemical Method for Structures, Vibrational Frequencies, and Noncovalent Interactions of Large Molecular Systems Parametrized for All Spd-Block Elements ( $Z = 1-86$ ). *J. Chem. Theory Comput.* **2017**, *13*, 1989–2009.
- [18] Bannwarth, C.; Caldeweyher, E.; Ehlert, S.; Hansen, A.; Pracht, P.; Seibert, J.; Spicher, S.; Grimme, S. Extended Tight-Binding Quantum Chemistry Methods. *Wiley Interdiscip. Rev. Comput. Mol. Sci.* **2021**, *11*.
- [19] Ess, D. H.; Houk, K. N. Distortion/Interaction Energy Control of 1,3-Dipolar Cycloaddition Reactivity. *J. Am. Chem. Soc.* **2007**, *129*, 10646–10647.
- [20] Bickelhaupt, F. M.; Houk, K. N. Analyzing Reaction Rates with the Distortion/Interaction-Activation Strain Model. *Angew. Chem. Int. Ed.* **2017**, *56*, 10070–10086.
- [21] Bickelhaupt, F. M. Understanding Reactivity with Kohn-Sham Molecular Orbital Theory: E2-SN2 Mechanistic Spectrum and Other Concepts. *J. Comput. Chem.* **1999**, *20*, 114–128.
- [22] Fernández, I.; Bickelhaupt, F. M. The Activation Strain Model and Molecular Orbital Theory: Understanding and Designing Chemical Reactions. *Chem. Soc. Rev.* **2014**, *43*, 4953–4967.
- [23] Wolters, L. P.; Bickelhaupt, F. M. The Activation Strain Model and Molecular Orbital Theory. *Wiley Interdiscip. Rev. Comput. Mol. Sci.* **2015**, *5*, 324–343.
- [24] Vermeeren, P.; van der Lubbe, S. C. C.; Fonseca Guerra, C.; Bickelhaupt, F. M.; Hamlin, T. A. Understanding Chemical Reactivity Using the Activation Strain Model. *Nat. Protoc.* **2020**, *15*, 649–667.
- [25] Wedi, P.; Farizyan, M.; Bergander, K.; Mück-Lichtenfeld, C.; van Gemmeren, M. Mechanism of the Arene-Limited Nondirected C–H Activation of Arenes with Palladium. *Angew. Chem. Int. Ed.* **2021**, *60*, 15641–15649.